11th International Symposium on Applications of Laser Techniques to Fluid Mechanics
Lisbon, Portugal, July 8-11, 2002

PIV/PLIF Investigation of Two-Phase Vortex-Flame Interactions

A. Lemaire,[1] T. R. Meyer,[2] K. Zahringer,[1] J. R. Gord,[3] and J. C. Rolon[1]

[1]*École Centrale Paris, Laboratoire d'EM2C*
Grande Voie des Vignes, 92295 Chatenay-Malabry Cedex, France

[2]*Innovative Scientific Solutions, Inc.*
2766 Indian Ripple Road, Dayton, OH 45440-3638, USA

[3]*Air Force Research Laboratory, Propulsion Directorate*
Wright-Patterson Air Force Base, OH 45433-7103, USA

ABSTRACT

The interaction between a vortex and a flat laminar diffusion flame is often used to simulate a number of features that are common in turbulent combustion, such as dynamic strain, stretch, and curvature. Using well-controlled experiments to verify numerical simulations, phenomena such as flame extinction and micro-vortex-flame behavior have been studied using gaseous fuels. The goal of this investigation is to study *two-phase* vortex-flame interactions using a number of laser diagnostic approaches, including particle-image velocity (PIV) and planar laser-induced fluorescence (PLIF). Data from CH PLIF diagnostics is effectively used to localize the diffusion flame front and extinction zones. In particular the evolution of flame surface area and rate of CH layer extinction as a function of time after vortex arrival is determined from PLIF images. Peak normal strain rates at extinction are calculated from PIV measurements. The evolution of the perturbed counterflow flame as a function of time after vortex arrival shows that micron-sized droplets strongly affect flame-surface development in the post-quenching stage of vortex-flame interaction. The relationship between peak normal strain rate and the time rate of CH layer extinction is also investigated by varying the vortex size and strength.

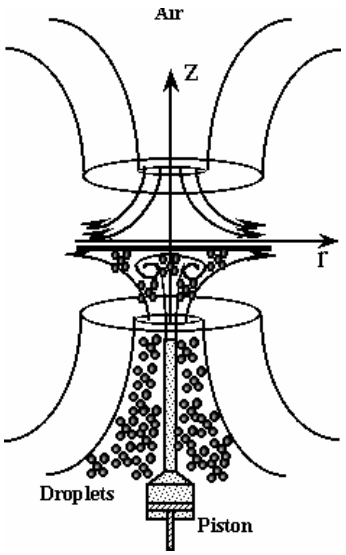

Flow Configuration.

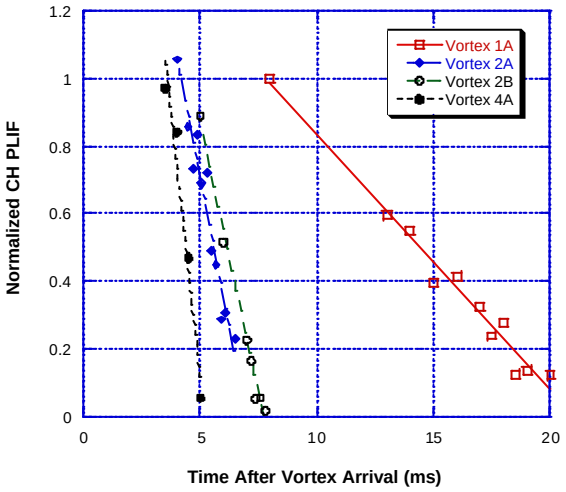

Rate of decay of CH mole fraction for different vortices.

1. Introduction

In the flamelet description of turbulent non-premixed combustion, local strain and curvature increase the scalar dissipation rate and can result in local flame extinction, reduced overall reaction rates, and decreased flame stability (Peters, 1986). A number of experimental studies have used well-controlled vortex injection to perturb steady H_2-air counterflow diffusion flames and simulate this unsteady local extinction process in a repeatable manner, as reviewed by Renard et al. (2000). These studies have been used to generate turbulent combustion diagrams (Thévenin et al., 2000), as well as to study the time evolution of surface area during gaseous vortex-flame interaction (Renard et al., 1999).

The goal of the current investigation is to study the extinction process during *two-phase* vortex-flame interaction. A flat non-premixed flame is established near the stagnation plane of a counterflow burner, and fuel-side vortices are introduced using an electronically actuated piston. The behavior of the reaction zone is studied using CH planar laser-induced fluorescence (PLIF), and vortex-induced strain is measured using particle-image velocimetry (PIV). Flame-surface evolution and relative CH mole fraction as a function of time relative to vortex perturbation are reported while varying the fuel composition, vortex size, and vortex strength. Results are presented for methane-air flames with and without the addition of n-heptane droplets.

The first studies of two-phase vortex-flame interactions in counterflow diffusion flames were reported by Santoro et al. (2000a and 2000b), who used methanol-air spray flames to avoid the effects of H_2 preferential diffusion and to capture flame phenomena found in practical devices. They compared vortex-induced perturbation and quasi-steady perturbation using PLIF of formaldehyde and laser Doppler velocimetry (LDV). They found that strain rates induced by air-side gaseous vortices are larger than quasi-steady strain rates by over a factor of two for a range of inlet oxidizer mass fractions. Santoro et al. (2000a and 2000b) did not vary the vortex properties, however, and did not introduce vortices on the droplet-laden fuel side as is done in the current investigation. The latter contribution is significant because of the prominence of fuel-side vortices in flame wrinkling and local extinction of turbulent diffusion flames (Watson et al., 1999).

Another important difference with previous investigations of single- or two-phase vortex-flame interactions is the use of CH planar-laser induced fluorescence in the current work. The CH radical has been widely used as a marker for the non-premixed flame zone because it appears in a narrow region of the flame near the location of peak temperature (Donbar et al., 2000; Han and Mungal, 2000). Unlike the premixed study of Nguyen and Paul (1996), measurements of OH and CH PLIF in turbulent diffusion flames indicate that CH does not exhibit “false” flame extinctions (Donbar et al., 2000). In the current investigation, CH PLIF is used both as a flame marker and as a measure of qualitative changes in the CH mole fraction during vortex-flame interaction. The latter is of interest because of the important role of CH in the formation of prompt NO and soot pollutants, and because of its role in NO_x reburning (Thoman and McIlroy, 2000). Qualitative measurements of CH mole fraction during vortex-flame interaction are also important for the optimization of multi-dimensional numerical simulations with complex chemical kinetic models.

2. Experimental Set-Up

2.1. Burner Apparatus

The experimental device used for this work was previously modified from a gaseous counterflow burner design (Rolon et al., 1991) to include a piston-actuated vortex injection system (Rolon et al., 1995). Details of this apparatus have been reported previously in the literature (Renard, et al., 1999; Fiechtner et al., 2000) and only a brief description is included here. As shown in Fig. 1, the burner consists two axisymmetric, 20-mm diameter counterflow nozzles, with air in the upper flow and a nitrogen-fuel mixture in the lower flow. A 40-mm diameter shroud flow of nitrogen surrounds each nozzle to shield the flame from ambient disturbances. The nozzle separation is set to 30 mm in this case. Vortex tubes of 2 mm and 3.7 mm are added along the centerline of the fuel nozzle, fed by an electronically controlled piston-actuation system. Vortices of varying strength are generated by controlling the size, stroke, and rise time of the piston. The resulting vortex circulation has been found to be equal to the square of the ejected fluid volume divided by

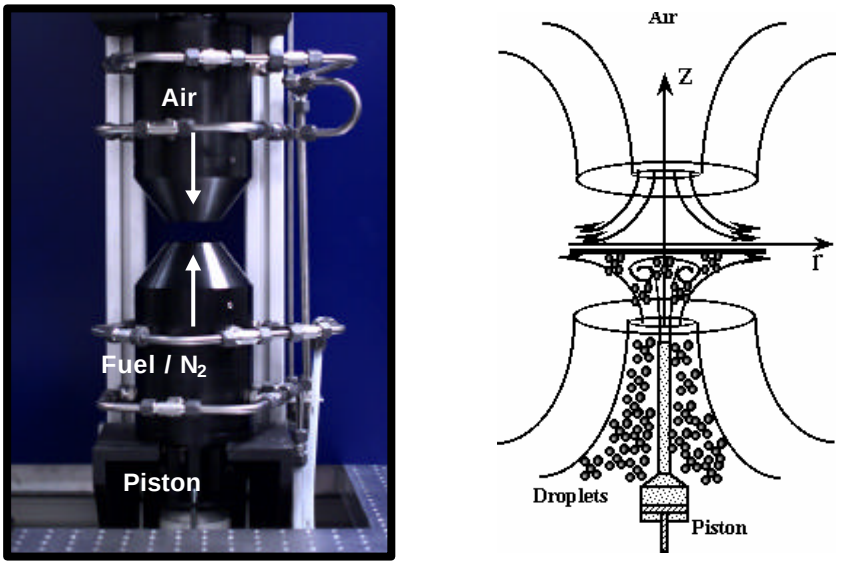

Fig. 1. Jet-in-co-flow burner used for vortex-flame experiments.

the piston rise time and the fourth power of the vortex tube diameter (Maxworthy, 1972). The vortex rotational and convection velocities have been found to be proportional to the circulation divided by the vortex-tube diameter (Roberts and Driscoll, 1991; Roberts et al., 1993). The relevant vortex properties for the current work are listed in Table 1. They include vortices with equal circulation but differing size and vortices with equal size but differing circulation.

The main modification to the burner apparatus for the current two-phase vortex-flame experiments is the addition of a nitrogen-jet atomizer in the fuel stream, described previously by Rolon et al. (1991) and similar to the apparatus characterized by Durox et al. (1999). This atomizer produces a mono-disperse field of droplets of about 2.43-2.83 μm in diameter for the current flow conditions. The spray is further diluted to a non-dense condition with methane and additional nitrogen to a volumetic density of 9×10^6 m^{-3}.

The various inlet flow conditions used in this investigation can be characterized by a number of parameters as listed in Table 1. They include the global mixture ratio, the steady nozzle velocities, v_{Ox} and v_{fuel}, and the ratio y between the mass of n-heptane droplets and the total mass of fuel. Cases A1 and A2 differ only in the inflow velocity and will be considered to be identical for the following discussion. Case B refers to a case with no n-heptane seeding but with total oxidizer and fuel mass fractions equal to that of Case A.

Table 1. Vortex properties and flow parameters used in the experiments.

Case	Vortex Tube Dia. (mm)	Piston Rise Time (ms)	Ejected Volume (mm^3)	Circulation (cm^2/s)	Meas. Peak Strain (/s)	Global Mixture Ratio	y	v_{Ox} (m/s)	v_{fuel} (m/s)
1A	3.7	10	37.9	7.7	750	4.43	0.57	0.7	0.5
2A	3.7	10	49.2	13	1573	4.43	0.57	0.7	0.5
2B	3.7	10	49.2	13	1363	4.43	0.0	0.7	0.5
3A	2	10	13.9	13	638	4.43	0.57	0.59	0.61
4A	2	10	37.9	90	1885	4.43	0.57	0.59	0.61

2.2. PIV System

PIV has been used in studies of premixed (Mueller et al., 1995) and non-premixed (Thévenin et al., 2000; Meyer et al., 2002) vortex-flame interactions to visualize the vortex flowfield and to determine the strain field acting on the flame. In the current study, digital cross-correlation PIV is achieved through Mie scattering from silicon-dioxide particles in the air stream and the n-heptane droplets in the fuel stream. The silicon dioxide is used due to its relatively low aggregate size (1-5 microns), high melting point (1700ºC), and porous structure. The use of Mie scattering of the n-heptane fuel droplets for PIV avoids problems with agglomeration of solid seed particles in the unvaporized fuel.

A double-pulsed Nd:YAG laser is used to generate overlapping 532-nm beams with 200 mJ of energy per beam. As shown in Fig. 2, the PIV beams are expanded in the vertical direction using a cylindrical lens (f=-12.7 mm) and are then recollimated using a spherical lens (f=500 mm). The PIV sheet thickness at the test section is approximately 0.5 mm. Pulse intervals are varied from 0.050 ms to 0.2 ms depending on the speed of the vortex, to keep particle displacements in a reasonable range. Dual-frame digital imaging of the two PIV signals is achieved using a 1008x1018 (9.07-mm x 9.16-mm) array Kodak Megaplus ES1.0 camera with 3.4x7 micron pixels. An AF Micro Nikkor 105 mm f/2.8 lens and a 36-mm extension ring are used to achieve a 2.2:1 image-to-CCD magnification ratio. Images are processed using custom designed software from Innovative Scientific Solutions, Inc. A 32x32 pixel interrogation region and 50% overlap is used to generate a 62x62 vector field across each image, and an adaptive mesh technique is used to obtain interrogation regions as small as 16x16 for calculations of peak strain rate.

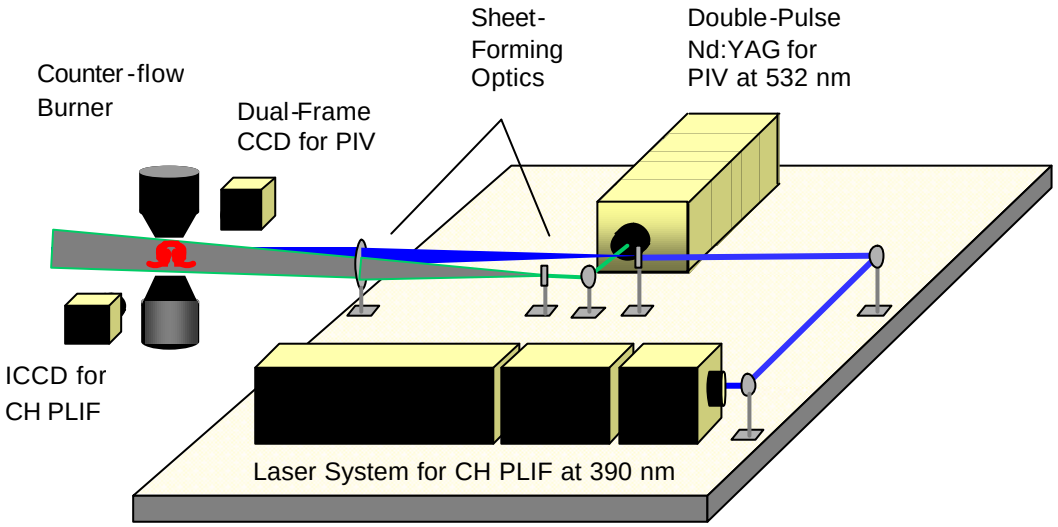

Fig. 2. Schematic of the simultaneous PLIF/PIV system.

2.3. CH PLIF System

The optical arrangement for CH detection by PLIF is also presented in Fig. 2. The laser system is composed of a Nd:YAG laser (1064 nm), doubled to 532 nm and pumping a tunable dye laser (Rhodamine 640). The dye-laser beam is frequency mixed with the Nd:YAG fundamental to obtain a wavelength corresponding to the $B^2\Sigma^- - X^2\Pi$ (0,0) absorption band between 388.5 and 391 nm. The $Q_1(5)$ transition of this band is excited at 389.5 nm. The laser system provides pulses of about 7 ns duration, whose mean energy is between 15 and 20 mJ. Fluorescence from the A-X (0,0) and A-X (1,1) bands was recorded to avoid interferences from background scattering.

After passing through two prisms, the beam is formed into a laser sheet by a cylindrical lens (f = 200 mm). This laser sheet is matched with the laser sheets from the PIV lasers in the spherical lens (f = 500 mm), which produces the parallel, superposed PIV and CH laser sheets in the center of the burner. The CH laser

sheet has a height of about 2 cm and a thickness of 0.3 mm. The energy distribution inside the CH laser sheet has been measured by Rayleigh scattering from nitrogen and Mie scattering from the droplets. The flame position is placed in the central region of the laser sheet, and the power density variation inside the region observed by the camera does not exceed 5%. In order to minimize further the effects of laser-sheet intensity variations, the laser fluence is adjusted so as to saturate the CH transition. As shown in Fig. 3, the CH PLIF signal is already in the saturated regime by about 4.5 MW/cm2 (1 mJ) and is near full saturation by 60 MW/cm2 (13 mJ).

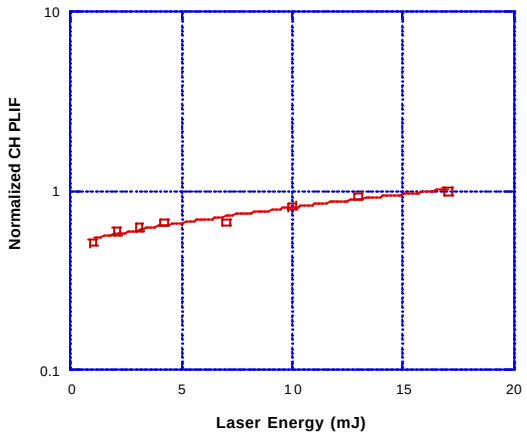

Fig. 3. CH PLIF intensity as a function of laser power. A nearly saturated regime is used in this study with laser powers between 15 and 20 mJ.

The CH PLIF signal is collected using a 512x512 array PI-Max intensified CCD camera with a 58-mm f/1.2 Noct-Nikkor lens. An image-to-CCD magnification ratio of 1.85:1 (imaged region of 20 mm x 20 mm) is achieved with a 20-mm extension ring. To improve signal-to-noise ratio, 2x2 binning of the CCD array is performed. The resulting limiting resolution based on the Nyquist criterion and modulation transfer function (MTF) of the lens is found to be about 234 microns. By definition, this is the smallest feature that the camera can distinguish. The CH-layer thickness (250 microns) is, therefore, fully resolved by the CH detection scheme. A combination of a 410-nm high-pass and a 450-nm low-pass filter are used to separate the CH LIF signal.

An important source of uncertainty in the CH signal during vortex-flame interaction arises from temperature-dependent fluorescence quenching rates. Based on results of a numerical simulation with complex chemistry, the main CH quenching species (H_2O, CO, N_2, and CO_2) are fairly constant in the region where CH is present. Quenching from O_2 and CH_4 nearly offset each other in the CH region, and temperature varies by less than 3%. Thus, the CH profile does not require significant corrections due to variation in temperature and quenching species. The variation of flame temperature during flame extinction can be significant, however, and must be considered. From 1700 K to 1100 K, the quenching cross-sections of H_2O, CH_4, and CO are expected to increase, while the quenching cross-sections of CO_2, N_2, and O_2 are expected to decrease (Tamura et al., 1997). After accounting for the temperature dependence of number density, the overall quenching rate of CH is estimated to decrease by about 10% during the flame-extinction process. The true effect of quenching variations is minimized by operating in the saturated regime. The decrease in CH fluorescence quenching and, thus, increase in fluorescence efficiency is augmented by a 25% increase in the Boltzman fraction of the $Q_1(5)$ rotational transition from 1700K to 1100K. This increases the detection limit of the experimental technique and ensures that "false" CH extinctions do not take place. Due to uncertainties in species mole fractions during flame extinction, however, the current technique underpredicts the true rate of strain-induced CH extinction. Full quantitative accuracy with temperature-dependent quenching corrections and measurements of species number density is beyond the scope of the current work and is currently being pursued in a parallel research program.

2.4. Synchronization System

Simultaneous CH PLIF and PIV diagnostics require precise synchronization of several events, including vortex generation, three laser pulses, and three camera exposures. The master delay generator is driven by the 10-Hz second pulse of the double-pulse PIV laser. It then triggers the piston driver, CH-PLIF laser system, and DANTEC PIV controller. The latter drives the PIV camera and lasers to ensure that all events occur simultaneously. The timing of the CH laser pulse occurs 20 μs before the second PIV laser pulse to avoid particle scattering. The vortex-flame interaction can be imaged at various phases of its development by adjusting relative timing of piston actuation and laser diagnostics. The initial time of the vortex-flame interaction is defined when the vortex starts to perturb the CH layer.

3. Results and Discussion

The velocity profile induced by Vortex 2A at 4.5 ms is shown in Fig. 4 (right). Note that the vectors are an average of five images and are presented in the reference frame of the vortex by subtracting a convection velocity of about 0.56 m/s. This frame of reference highlights the circulating flow pattern and makes it easier to determine the vortex position as a function of time. Since flame extinction in the current experiments is observed to take place at the centerline, the relevant normal strain rate induced by the vortex is defined as dv/dz, where v is the vertical component of velocity and z is the axial coordinate. The peak fuel-side normal strain rate of about 1750 s^{-1} occurs near the stagnation point in the convective frame of reference. Figure 4 demonstrates the ability of the current technique to measure the normal strain rate along the entire axis as a function of time. Adequacy of PIV resolution is demonstrated as the strain rate is found to be "grid independent" for interrogation regions of 32x32 or less. Results from calculations of other vortices are shown in Table 1.

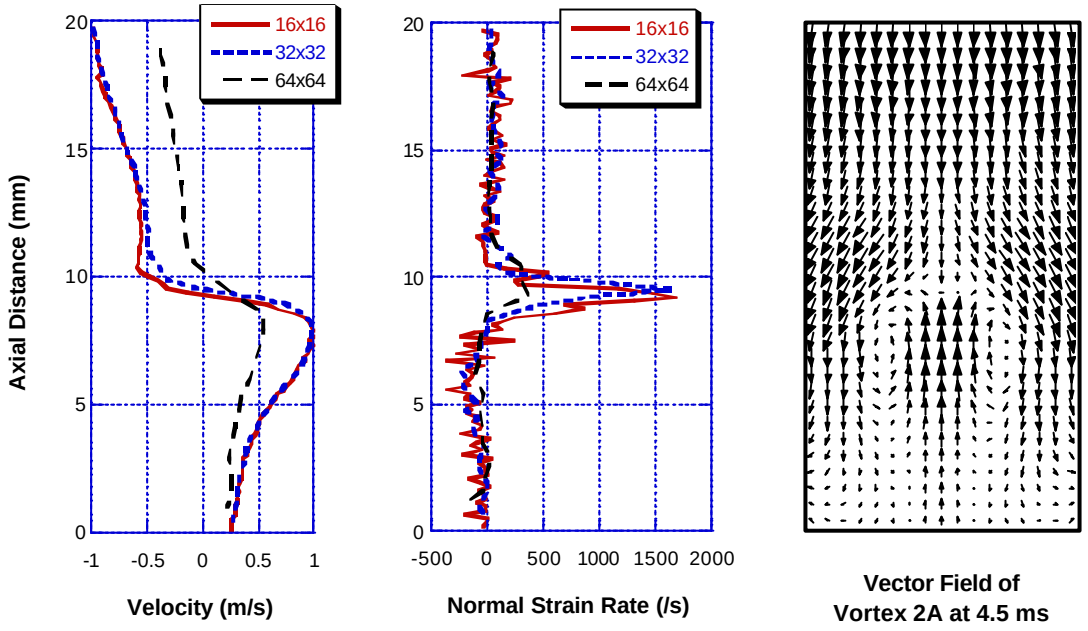

Fig. 4. Comparison of velocity and normal strain rate for Vortex 2A using different PIV interrogation regions. Interrogation regions of 32x32 pixels (3 vectors/mm) or 16x16 pixels (6 vectors/mm) are shown to be adequate for computing peak strain rates. Overlap parameter is 50%.

The time evolution of the perturbed counterflow flame as a function of time after vortex arrival is shown in Fig. 5 for Vortex 2A. The CH layer is located above a strong fluorescence signal from species on the fuel-side of the flame. Based on a numerical simulation with complex chemistry, this layer of fluoresecence corresponds to the location of polycyclic aromatic hydrocarbons (PAH). Interference from this layer is minimized by spatial separation with CH, as shown in Fig. 5, and by the fact its fluorescence is strongly dimished by the approaching vortex. In describing the evolution of the CH layer in Fig. 5, time zero is defined as the time at which the vortex starts to perturb the counterflow flame. At 4.5 ms, the flame is clearly wrinkled but has not yet been extinguished. By 5.3 ms, the flame is clearly descreasing in intensity at the centerline, but does not seem to change in width. Extinction is fully established by 5.7 ms, allowing the droplet-laden vortex to continue past the flame. A slight outline of the vortex is visible at 23 ms due to Mie scattering.

In order to obtain qualitative information about the effects of the vortex on the flame, one can calculate the time evolution of the flame surface and CH-layer centerline intensity from experimental images. Data from CH PLIF diagnostics effectively localize the diffusion flame front and extinction zones (extinction signal refers to signal that falls to the background noise). One can define the flame front position by following the

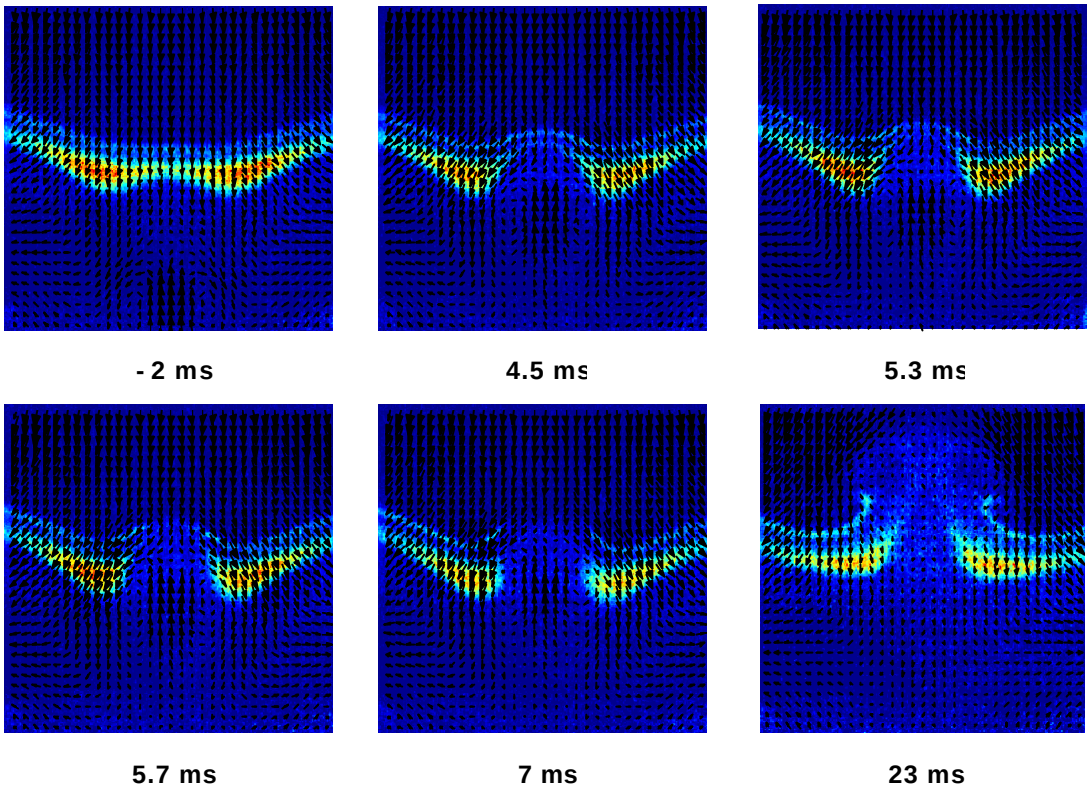

Fig. 5. Sample CH PLIF / PIV sequence of Vortex 2A showing the vortex-flame interaction at various phases of evolution. Times are relative to when the vortex first wrinkles the flame.

maxima of CH intensity for an average of ten images (two symmetric halves per image) while avoiding high intensity pixels due to PAH signal. Once the flame front is determined, each segment between two points is treated as an elementary area and is rotated about the axis of symmetry using the Guldin theorem. The total flame surface is a sum of the elementary areas and is normalized by the value of the non-perturbed flame.

The evolution of flame surface area as a function of time after vortex arrival is shown in Fig. 6 for several vortex and flow configurations listed in Table 1. In Cases 2A and 4A, extiction starts after about 5 ms and results in a strong descrease in flame surface area. This decrease is followed by a plateau between 7 and 16 ms and an increase after 18 ms. The latter is not due to reconnection, but occurs because the edges of the flame are entrained by the vortex after extinction, thereby increasing the total surface area. The larger vortex of Case 2A results in a stronger decrease in flame surface area during extinction. Case 2B, where the flame is not doped by n-heptane droplets, does not show the constant plateau, and the flame surface area continues to decrease. This can be explained by the excess of unburned n-heptane

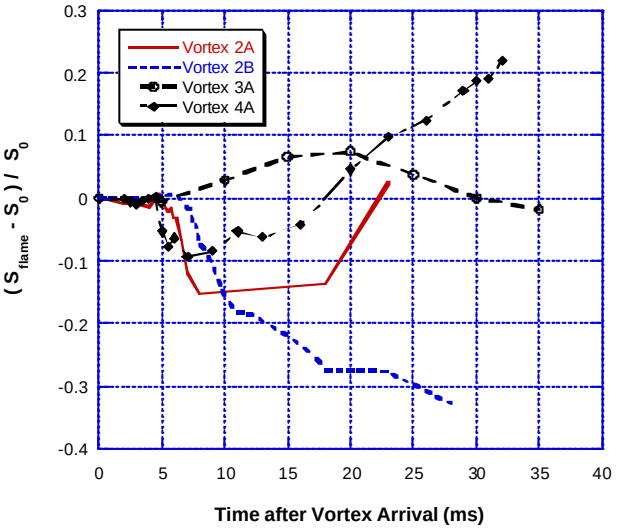

Fig. 6. Evolution of normalized flame-surface area during vortex-flame interaction. Vortex and flame conditions refer to Table 1.

droplets in Case 2A, which evaporate and contribute to the formation of a cylindrical flame around the axis. No extinction takes place for the smaller vortex of Case 3A, despite having similar vortex circulation and higher vortex velocity than Case 2A (recall, vortex rotational and convection velocity ~ circulation / tube diameter). Thus, the flame surface area increases in Case 3A due to flame wrinkling and decays back to its original level after the vortex is dissipated. The explanation for the lack of extinction in Case 3A is partially related to the vortex size. The tangential velocity of the larger vortex is higher, thus increasing the strain rate at the flame surface and increasing the likelihood of extinction. In addition, the larger vortex is less dissipated by heat release and is better able to sustain high levels of strain. Case 3B can be contrasted with 4A, which has the same vortex size as 3A but experiences flame extinction due to signitificantly higher vortex circulation and velocity.

In addition to flame surface area, the *rate* of flame extinction provides another means of evaluating the effects of fuel composition and vortex strength. Figure 7 plots the centerline peak CH intensity as a function of time during the extinction process for Cases 1A, 2A, 2B, and 4A, and indicates that the process is nearly linear with respect to time. The slowest rate of extinction is achieved in Case 1A (slope = 0.076), which has the lowest value of circulation but has a large enough vortex to extinguish the flame. Consistent with the early evolution of flame surface area, shown previously in Fig. 6, Case 2A with droplets extinguishes earlier and slightly faster (slope = 0.350) than Case 2B without droplets (slope = 0.317). Case 4A has the highest cirulation and vortex velocity and also has the highest rate of extinction (slope = 0.625). This behavior is consistent with the measured peak normal strain rates shown in Table 1. It is worth noting, however, that the peak normal strain rates for Cases 3A and 4A (2-mm vortex tube) have much lower strain rates than expected based on the theoretical value of circulation (Table 1). As alluded to earlier, this may be due to the higher level of energy dissipation experienced by smaller vortices.

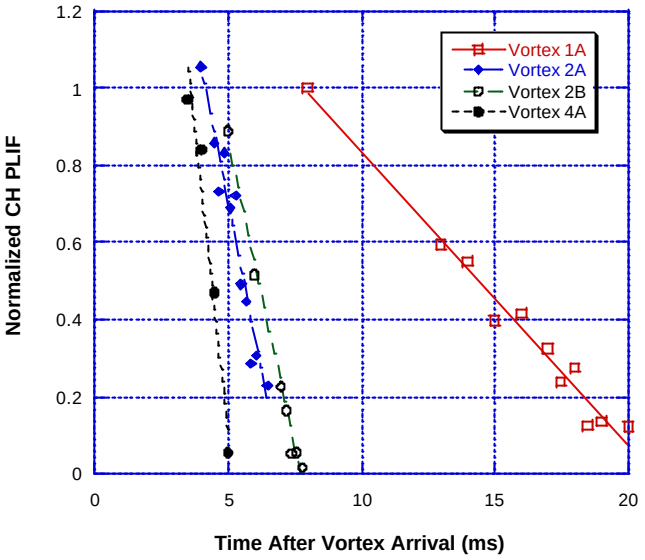

Fig. 7. Relative CH mole fraction during flame extinction.

4. Conclusions

The interaction between a vortex and a two-phase non-premixed flame has been studied using CH PLIF and PIV. Analyses of interferences from PAH and the temperature-dependent CH fluorescence efficiency indicate that the CH LIF signal qualitatively tracks the CH mole fraction. Using an adaptive mesh technique, the PIV system was shown to have adequate resolution for measurements of peak normal strain during vortex-flame interaction. We deduced from these measurements the vortex-induced time evolution of single- and two-phase counterflow diffusion flames.

The results of the present investigation show that micron-sized droplets convected by vortices strongly affect the post-extinction flame-surface development of counterflow diffusion flames. Unlike previous studies with larger droplets (~ 40 microns), the current work (~ 2-3 microns) showed only moderate effects on the timing and rate of flame extinction. The effects of vortex size and velocity were also studied in the context of flame surface area evolution and flame extinction. The flame experiences rapid extinction for vortices of high velocity and strength due to increased normal strain rates. Recovery of flame surface area occurs more quickly for smaller vortices, however, due to flame propagation along the vortex column after the extinction event.

Based on this investigation, CH PLIF and PIV have been shown to be excellent techniques for evaluating vortex-induced flame perturbations in hydrocarbon-air systems. The rate of CH extinction can be described conveniently by a single value since the drop in CH mole fraction is found to be a linear function of time (after a short transient) for a variety of conditions. Future work on the current data set includes processing of a wider range of fuel compositions and vortex conditions for the development of combustion diagrams and for extraction of more conclusive empirical trends.

Acknowledgments

The authors would like to acknowledge the help and advice of Dr. V. R. Katta of Innovative Scientific Solutions, Inc., and Dr. C. D. Carter of the Air Force Research Laboratory. This work was supported by U.S. Air Force Contract F33615-00-C-2068 and French DGA / ONERA PEA -number 98703-TITAN in a French-U.S. collaborative program.

References

Donbar, J. M., Driscoll, J. F., and Carter, C. D. (2000), "Reaction Zone Structure in Turbulent Nonpremixed Jet Flames - From CH-OH PLIF Images," *Combustion and Flame* 122:1-19.

Durox, D., Ducruix, S., and Lacas, F. (1999), "Flow Seeding with an Air Nebulizer," *Experiments in Fluids* 27:408-413.

Fiechtner, G. J., Renard, P. H., Carter, C. D., Gord, J. R. and Rolon, J. C. (2000), "Injection of Single and Multiple Vortices in an Opposed-Jet Burner," *Journal of Visualization* 2:331-341.

Han, D. and Mungal, M. G. (2000), "Simultaneous Measurement of Velocity and CH Layer Distribution in Turbulent Non-Premixed Flames," *Proceedings of the Combustion Institute* 28:261-267.

Maxworthy, T. (1972), "The Structure and Stability of Vortex Rings," *Journal of Fluid Mechanics* 51:15-32.

Meyer, T. R., Fiechtner, G. J., Gogineni, S. P., Rolon, J. C., Carter, C. D., and Gord, J. R. (2002), "PLIF/PIV Study of Vortex-Induced Annular Extinction in Counterflow H2-Air Diffusion Flames," Submitted for Publication, *Experiments in Fluids*.

Mueller, C. J., Driscoll, J. F., Sutkus, D. J., Roberts, W. L., Drake, M. C., and Smooke, M. D. (1995), "Effect of Unsteady Stretch Rate on OH Chemistry during a Flame-Vortex Interaction: To Assess Flamelet Models," *Combustion and Flame* 100:323-331.

Nguyen, Q. V. and Paul, P. H. (1996), "The Time Evolution of a Vortex-Flame Interaction Observed Via Planar Imaging of CH and OH," *Proceedings of the Combustion Institute* 26:357-364.

Peters, N. (1986), "Laminar Flamelet Concepts in Turbulent Combustion," Twenty-First Symposium (International) on Combustion, The Combustion Institute, pp. 1231-1250.

Renard P. H., Rolon, J. C., Thévenin, D., and Candel, S. (1999), "Investigations of Heat Release, Extinction, and Time Evolution of the Flame Surface for a Non-Premixed Flame Interacting with a Vortex," *Combustion and Flame* 117:189-205.

Renard, P. H., Thevenin, D., Rolon, J. C. and Candel, S. (2000), "Dynamics of Flame/Vortex Interactions," *Progress in Energy and Combustion Science* 26:225-282.

Roberts, W. and Driscoll, J. (1991) *Combustion and Flame* 87:245-256.

Roberts, W., Driscoll, J., Drake, M., and Goss, L. (1993), *Combustion and Flame* 94:58-69.

Rolon, J. C., Aguerre, F. and Candel, S. (1995), *Combustion and Flame* 100: 422-429.

Rolon, J. C., Veynante, D., Martin, J. P., and Durst, F. (1991), "Counter Jet Stagnation Flows," *Experiments in Fluids* 11:313-324.

Santoro, V. S., Kyritsis, D. C., Linan, A., and Go mez, A. (2000a), "Vortex-Induced Extinction Behavior in Methanol Gaseous Flames: A Comparison with Quasi-Steady Extinction," *Proceedings of the Combustion Institute* 28:2109-2116.

Santoro, V. S., Kyritsis, D. C. and Gomez, A. (2000b), "An Experimental Study of Vortex-Flame Interaction in Counterflow Spray Diffusion Flames," *Proceedings of the Combustion Institute* 28:1023-1030.

Tamura, M., Berg, P. A., Harrington, J. E., Luque, J., and Jeffries, J. B., Smith, G. P., and Crosley, D. R., "Collisional Quenchin g of OH, CH, and NO in Low Pressure Flames," Western States/The Combustion Institute Spring Technical Meeting, Livermore, California, 1997.

Thévenin, D., Renard, P. H., Fiechtner, G. J., Gord, J. R., and Rolon, J. C. (2000), "Regimes of Non-Premixed Flame-Vortex Interactions," *Proceedings of the Combustion Institute* 28:2101-2108.

Thoman, J. W. and McIlroy, A. (2000), "Absolute CH Radical Concentrations in Rich Low-Pressure Methane-Oxygen-Argon Flames via Cavity Ringdown Spectroscopy of the A2D-X2P Transit ion," *Journal of Physical Chemistry A* 104:4953-4961.

Watson, K. A., Lyons, K. M., Donbar, J. M., and Carter, C. D. (1999), "Scalar and Velocity Field Measurements in a Lifted CH4-Air Diffusion Flame," *Combustion and Flame* 117:257-271.